Received: 19 April 2023 | Revised: 17 April 2024 | Accepted: 21 May 2024

DOI: 10.1002/jez.b.23267

RESEARCH ARTICLE

JEZ-B MOLECULAR AND DEVELOPMENTAL EVOLUTION WILEY

A microfluidic chip for immobilization and imaging of *Ciona intestinalis* larvae

Guillaume Poncelet[1] | **Lucia Parolini**[2] | **Sebastian M. Shimeld**[1]

[1]Department of Biology, University of Oxford, Oxford, UK

[2]Peter Medawar Building for Pathogen Research, Nuffield Department of Medicine and Physical and Theoretical Chemistry Laboratory, Department of Chemistry, University of Oxford, Oxford, UK

Correspondence
Sebastian M. Shimeld, Department of Biology, University of Oxford, 11a Mansfield Rd, Oxford OX1 3SZ, UK.
Email: sebastian.shimeld@biology.ox.ac.uk

Funding information
John Fell Fund; Elizabeth Hannah Jenkinson Fund; University of Oxford

Abstract

Sea squirts (Tunicata) are chordates and develop a swimming larva with a small and defined number of individually identifiable cells. This offers the prospect of connecting specific stimuli to behavioral output and characterizing the neural activity that links these together. Here, we describe the development of a microfluidic chip that allows live larvae of the sea squirt *Ciona intestinalis* to be immobilized and recorded. By generating transgenic larvae expressing GCaAMP6m in defined cells, we show that calcium ion levels can be recorded from immobilized larvae, while microfluidic control allows larvae to be exposed to specific waterborne stimuli. We trial this on sea water carrying increased levels of carbon dioxide, providing evidence that larvae can sense this gas.

KEYWORDS
carbon dioxide, *Ciona*, microfluidic, neuron, olfaction

1 | INTRODUCTION

Two closely related species of sea squirt, *Ciona intestinalis* and *Ciona robusta*, are widely used in developmental and evolutionary biology. Fertilization in *Ciona spcs*. occurs in the water column following broadcast spawning, and embryos undergo a deterministic developmental program resulting in larvae with a small and defined number of cells (Imai & Meinertzhagen, 2007; Nicol & Meinertzhagen, 1991). *Ciona spcs*. larvae are motile and integrate environmental cues to identify an appropriate site for settlement and metamorphosis (Pennati et al., 2009). Larvae can respond to light and gravity through sensory cells embedded in the anterior swelling of the central nervous system known as the sensory vesicle (Figure 1a,b; Bostwick et al., 2020; Kourakis et al., 2019; Tsuda et al., 2003). Larvae also possess a small number of sensory cells in the epidermis (Figure 1c; Imai & Meinertzhagen, 2007; Yokoyama et al., 2014). These include neurons in the tail (DCENs, VCENs, and BTNs: see Figure 1), ciliated neurons dorsal to the sensory vesicle known as the anterior apical trunk epidermal neurons (aATENs) and posterior apical trunk epidermal neurons, neurons embedded in the three anterior projections known as palps or papillae (palp sensory neurons [PSNs]), and the rostral trunk epidermal neurons (RTENs) that link the palps to the sensory vesicle. The aATENs and PSNs have been proposed to be chemosensory neurons (Abitua et al., 2015; Poncelet & Shimeld, 2020) and palps have been shown to be mechanosensory (Wakai et al., 2021). Palps contain two other cell types in addition to PSNs, central collocytes and axial columnar cells (ACCs; Figure 1c). ACCs have also been suggested to be chemosensory (Johnson et al., 2020; Zeng et al., 2019). Larval behavior and ecology suggest that *Ciona spcs*. larval chemosensation is likely to include sensation of biofilm-derived chemical cues for selecting an appropriate settlement site (Hadfield, 2011). It may also include sensation of dissolved gasses such as carbon dioxide (CO_2) as this ability is widespread in living organisms (Jones, 2013; Scott, 2011). However, to date, gas sensing has not been experimentally demonstrated for any *Ciona spcs*. cells.

Here, we report the development of methodology for live calcium ion (Ca^{2+}) imaging in *C. intestinalis* larvae exposed to a controlled chemical stimulus. Previous studies have demonstrated the activity of the Ca^{2+} reporter GCaMP in *Ciona spcs*. following injection of *GCaMP* messenger

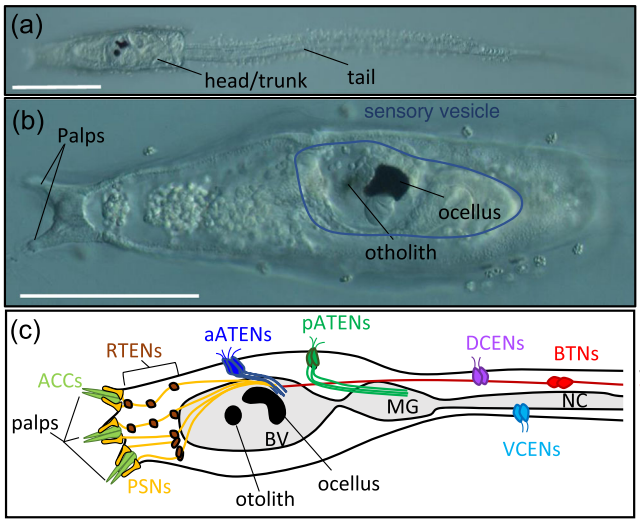

FIGURE 1 *Ciona* larva neural anatomy. (a) Motile *Ciona intestinalis* larva at 22 h postfertilization (hpf). Note that the head of a *Ciona* tadpole larva is usually called the "trunk" in literature on this species. Both terms are used in this figure, but the trunk is used in the text. (b) Head/trunk of larva at 22 hpf with palps, otolith, and ocellus labelled. The approximate outline of the sensory vesicle is shown in blue. (c) Schematic drawing of larval head/trunk showing the various epidermal sensory cells: bipolar tail neurons, dorsal and ventral caudal epidermal neurons, anterior and posterior apical trunk epidermal neurons, rostral trunk epidermal neurons, and the palp sensory neurons and axial columnal cells. Scale bars: (a) 100 µm and (b) 50 µm.

RNA (mRNA) or electroporation of GCaMP-encoding plasmids (Abdul-Wajid et al., 2015; Akahoshi et al., 2017; Hackley et al., 2013; Kolar et al., 2021; Okawa et al., 2020; Wakai et al., 2021). In principle, this approach should allow imaging of individual cells while animals are exposed to defined stimuli, and significant steps have been made toward these goals with activities traced to identified cells and the development of an integrated computational platform to support experiments and analyses (Akahoshi et al., 2017; Kolar et al., 2021). A major challenge remains the motility of the larvae: larvae swim vigorously making imaging of free-range larvae challenging. Anesthetics may block this behavior but may also compromise neural responses and hence experimental outcomes. Other forms of immobilization are necessary if imaging is to link controlled sensory stimulation to neural and behavioral response. We here report the development of a microfluidic chip that allows *C. intestinalis* larvae to be immobilized and imaged while exposed to potential olfactants. We couple this with the deployment of a transgenic GCaMP system in which the reporter protein is expressed in a small subset of cells and use this to record responses to dissolved CO_2.

2 | RESULTS

2.1 | Live cell reporting in *C. intestinalis* larvae

We first sought proof of principle for Ca^{2+} detection with genetically encoded GCaMP6m in live *C. intestinalis* larval trunks. We selected a GCaMP6 because *GCAMP6s* mRNA has been used successfully by injection in *Ciona spcs*. (Akahoshi et al., 2017) and *Platynereis* (Chartier et al., 2018) and we specifically selected GCaMP6m because it has a faster kinetic response (Chen et al., 2013). We targeted GCaMP6m to a defined part of the trunk using the *C. robusta DMRT* regulatory region (Wagner & Levine, 2012), which is expressed in rows III and VI of the neural plate at the mid-gastrula stage. Rows III and IV contribute to the central nervous system (CNS), including the anterior sensory vesicle, while rows V and VI contribute to the palps, oral siphon primordium, and peripheral nervous system (Gainous et al., 2015; Tresser et al., 2010). To determine whether this construct was expressed in the correct cells in the trunk, we imaged multiple larvae revealing transgene expression as previously reported, though we also noted occasional fluorescent cells in the tail and that sometimes fluorescent debris stuck to larvae (examples are provided in Figure S1).

To determine if fluorescence could be seen and recorded responding to cytosolic Ca^{2+} change, *C. intestinalis* larvae transgenic for *DMRT>GCaMP6m* were immobilized in low-melting-point agarose in a perfusion slide and fluorescence recorded before and after the addition of the calcium ionophore A23187. Before the addition of the ionophore, fluorescence could be seen in some of the cells we expected the *DMRT* regulatory region would target, including in the palps and the CNS (Figure 2a), although some ectopic expression was seen in other tissues as is common with transgenesis in these species. After the addition of A23187, fluorescence was visible more broadly, especially in the palps (Figure 2b). This experiment demonstrated that GCaMP6m could be delivered to appropriate cells, was regulated by the calcium ionophore, and that fluorescence could be recorded in live animals. We hence concluded that the method could be used for live imaging of endogenous calcium levels in these cell populations.

2.2 | Chip design and equipment organization

Printed chips and microfluidics have been used to study behavior in other marine larvae (Chartier et al., 2018), but not to our knowledge for tunicate larvae in a chip designed for microfluidic exposure to odorants. Our first step was to identify the relevant dimensions to trap live *C. intestinalis* larvae. The larval trunk is the widest part of the body and measurements of 50 larvae revealed that the maximum trunk width was about 89 µm (with a standard deviation of 10 µm, 95% confidence interval bounds 82.15–95.7 µm). We trialled a modification of the chip design developed for immobilization and imaging of larvae of the polychaete *Platynereis* (Chartier et al., 2018). This consisted of a trapping channel with a constant height of 60 µm and a width that decreased linearly along its main axis from 150 to 80 µm. While this design proved suitable for loading and initial containment of larvae, flow pressure caused larvae to be pulled back into the introduction channel or beyond the trapping zone. This is because the trunks of *C. intestinalis* larvae can be deformed by pressure and lack the chaetae of polychaete larvae, which may help them lodge in position.

To circumvent these limitations, we trialled a variety of chip designs before settling on a symmetrical chip organized around a

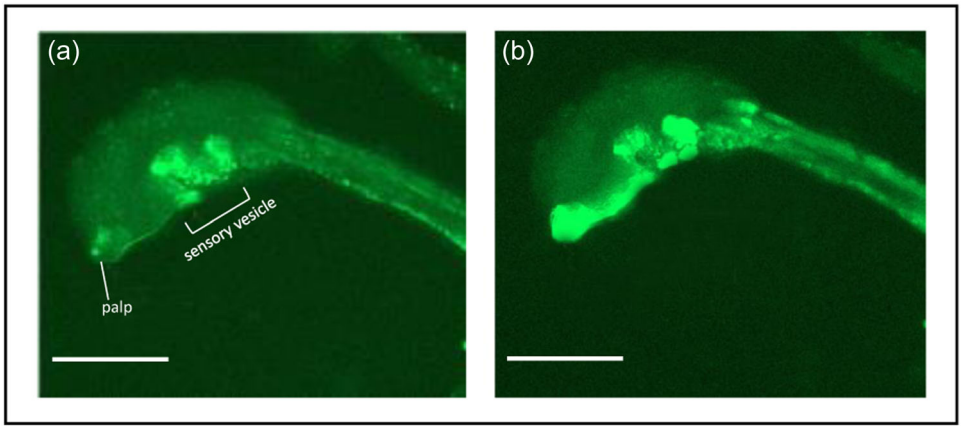

FIGURE 2 Validation of GCaMP6m fluorescence in transgenic *Ciona intestinalis*. (a) Larva perfused with sea water and (b) sea water with 1 M Ca^{2+} ionophore A23187. Note that these images were obtained using a different experimental setup to those in Figure 7, so the fluorescent intensity is not directly comparable between these figures. Also, note that in (a) only one palp is visibly labelled with fluorescence, meaning the other two are not discernible. In this individual, the construct also shows some ectopic expression in the tail. Scale bars = 100 µm. Additional larvae expressing this transgene are shown in Figures S1 and S2.

central trapping channel of width 500 µm, length 2 cm, and height 23.5 µm, which holds the animals dorsoventrally (Figure 3 and Additional File S1). An animal introduction inlet is situated in the middle of the trapping channel. Immobilization works primarily through dorsoventral compression: to determine the height of the channel, we started with the design of Cartier et al., then reduced the height in decrements of 5, 1, 0.5 µm, arriving at 23.5 µm by this empirical process. The chip includes three inlet channels that deliver the test solutions into a chamber upstream of the trapping channel, which has a width of 2 mm. This splits into the trapping channel plus two lateral channels with a width of 1 mm each. These come back together at the back of the chip where one outlet channel is sited. This chip allows the introduction, immobilization, and recording of multiple animals at the same time. We also noted that aspects of the chip design of Chartier et al. (2018) were enhancing the trapping of air bubbles, which may affect fluid flow behavior (Figure 3b). Bubbles can be removed by degassing; however, this was not desirable here as the stimulus to be tested was also a gas. This issue was resolved by altering the chip design to make some surfaces triangular instead of flat (Figure 3c). This did not affect the smooth transition of flow boundaries, but bubbles in the chip were flushed out by the fluid flow without further intervention. A limitation of the design is that larvae are held firmly in position: while this is necessary for imaging, a consequence is that behaviors like tail movements (Athira et al., 2022) are difficult to see.

A customized 3D-printed chip holder (Additional File S2) was used to maintain the chip under an upright microscope. Inlet pressure was controlled using an MFCS™-EZ (Fluigent) having an integrated positive pressure source with three pressure channels with ranges from 0 to 345 mbar (0–34.5 kPa). This was connected to a computer running the Fluigent Microfluidic Automation Tool which controlled flow rates in each channel. Each channel was drawn from a separate tube filled with a test solution. The MFCS™-EZ was positioned next to the microscope stage, with a constant tubing length of 30 cm used to connect tubes and chips. Equipment organization can be seen in Figure 4. The electroporated transgenic larvae were introduced into the chip by sucking them into a polytetrafluorethylene tube plugged to a metallic needle (Mircolance #20, 302200; BD) connected to a plastic syringe (Luer Plastipak). The animals inside the tube were fed into the introduction inlet by applying light pressure on the plastic syringe to slowly push them inside the trapping channel. To understand the impact of introduction into the chip on larval morphology, we imaged larvae with bright field and *DMRT>GCaMP6m* fluorescence before and after the process (Figure S2). We noted that chip introduction could cause mechanical distortion of the trunk though this was variable between individuals.

2.3 | Chip calibration

Calibration recordings were done with a Carl Zeiss Axioskop 2 plus microscope mounted with a Zeiss AxioCam HRc camera. Fast Green FCF (E143) was dissolved at 0.5 g mL^{-1} in the two side streams to visualize their moving boundaries (Figure 5) (video recording in Additional File S3, see Data availability and Section 4 below for details). A single frame was taken every 6.8 ms. The mean gray value through all frames was calculated using Fiji, in a square ROI, of constant in size and position, located in the trapping channel. Minimal and maximal pixel values, which according to the Beer–Lambert law corresponded, respectively, to the absence of Fast Green FCF and its maximum concentration, were normalized between 0 and 1 (Figure 5). To assess the reproducibility of flow onset and offset, measurements were made successively 60 times and these data were superimposed (Figure 5). This revealed that the onset took 390 ms on average with a duration variability of 197 ms. The offset took around 27 ms, with no detectable variability in duration. The experiment demonstrated the reproducibility of the stimulation onset/offset. Once these conditions for boundary control were established, the dye was no longer used.

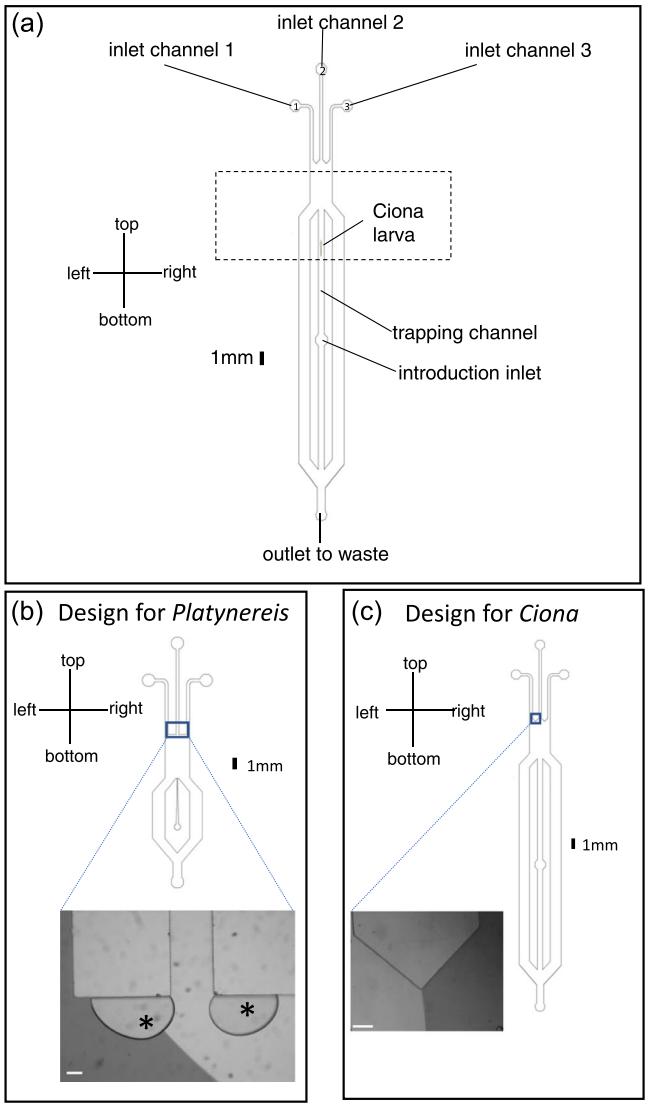

FIGURE 3 Microfluidic chip design used in this study. (a) Overview of chip design. Scale bars = mm. The dashed box outlines the approximate area shown in Figures 5 and 6. (b) The chip design of Chartier et al. (2018) for *Platynereis* traps air bubbles visible on the photograph (black asterisk) on flat surfaces located before the main chamber. (c) In the modified design used in this study, the surfaces are triangular instead of flat, precluding bubble retention. In (b and c), fluid flow is from top to bottom in the pictures, and the flow boundary is visible as one stream is labelled with fast green (dark gray) and the other is unlabelled water (light gray). Scale bars on the diagrams are 1 mm as indicated, and scale bars on the photographs are 100 µm. The design file is available as Additional File S1.

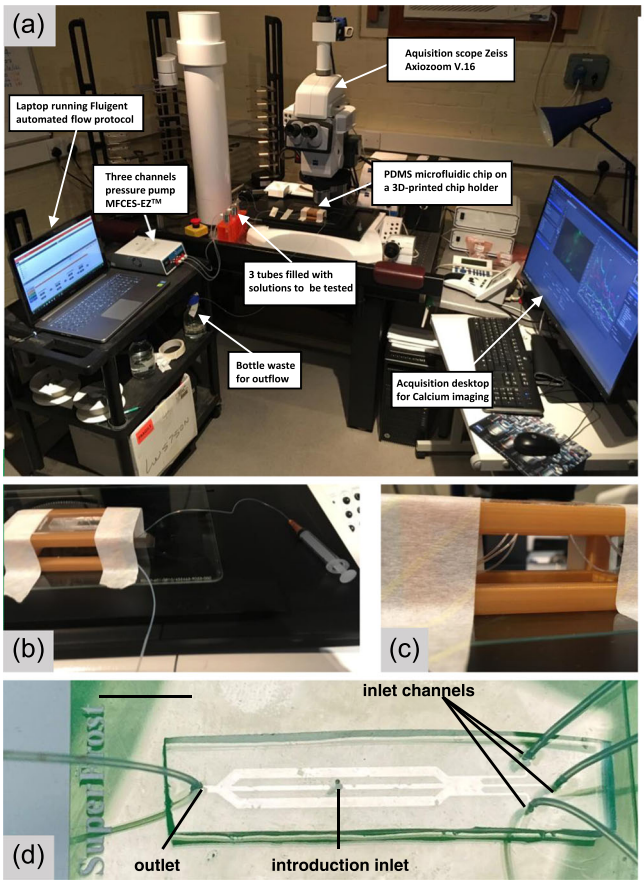

FIGURE 4 Experimental setup for live animal imaging. (a) The controller MFCES-EZ™ with three pressure channels on the left side of a Fluorescence Stereo microscope Zeiss Axio Zoom V.16. Each pressure channel operates a tube connected to an inlet of the chip. The bottle on the left bottom is for collection of the outflow. (b) The customized three-dimensional-printed chip holder (golden color) holding the polydimethylsiloxane microfluidic chip with tape. The syringe visible on the right side of the microfluidic chip is used for animal introduction. (c) The three inlet tubes are visible on the left side, while the introduction and outlet tubes are visible on the right side. (d) Photograph of the chip with inlets and outlets identified, and lit so that the internal design is visible. Scale bar on (d) is 1 cm.

2.4 | Establishing laminar flow and testing the response to CO_2

Calcium recordings were conducted on 20–24 h postfertilization (hpf) *C. intestinalis* larvae at room temperature. Electroporation-induced transgenesis has the potential to cause developmental anomalies. To mitigate this, we scrutinized all transgenic larvae using a dissecting microscope before their introduction into the chip, selecting only those exhibiting typical morphology and swimming patterns. Consequently, any observed deformations in the imaged larvae, such as tails encircling the trunk, can be attributed to mechanical influences during the loading and immobilization process rather than genetic manipulation. For these experiments, we maintained a total pressure of 200 mbar (20 kPa) in the chip at all times, with the central inlet at 80 mbar (8 kPa) and left and right channels at 0 or 120 mbar (0–12 kPa) (Figure 6). This allowed a controlled transition between exposure to central or lateral streams. One lateral stream contained a high CO_2 stimulus solution (S) and the other a pH-matched control (C) of sea water with a corrected pH value equivalent to that of the high CO_2 solution. In total seven larval trunks were imaged (Figures 7 and S3). Parts of the trunk were designated as ROIs. To define these, we first examined recordings by eye in Fiji, looking

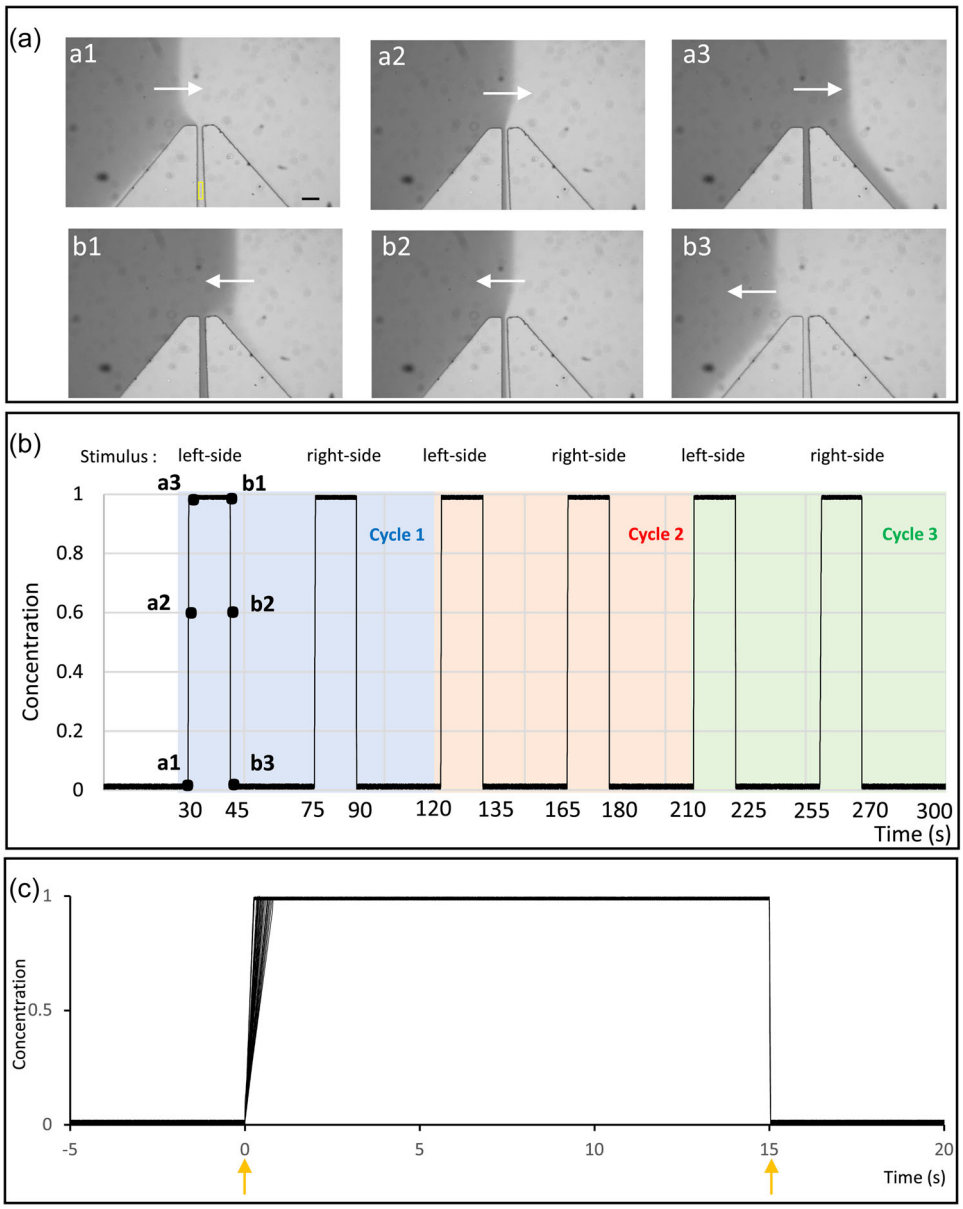

FIGURE 5 Calibration experiment to measure the temporal variations of stimulus concentration. (a) The pictures illustrate the consecutive steps during onset (a_1, a_2, and a_3) and offset (b_1, b_2, and b_3) of the stimulus located on the left side of the trapping channel. The flow moves from top to bottom and the arrow indicates the horizontal movement of stream boundaries, visualized with a dye. The scale bar on (a1) is 1 mm and applies to all six images. (b) Graph representing the normalized stimulus concentration estimated from mean gray value intensity measured in a region of interest inside the trapping channel (yellow rectangle shown in a1). The graph represents the entire experimental flow protocol used during one calibration experiment. The trapping channel is exposed to either left-side stimulus or right-side stimulus for 15 s with resting intervals of 30 s during three repetitive cycles (blue, red, and green). (c) Graph representing all 60 measurements of onset/offset with the different cycles and stimulus sides together. The normalized stimulus concentration (from 0 to 1) is estimated from the mean gray value intensity. The orange arrows indicate the time point when the pressure controller switches pressure rates starting at Time 0 and ending at Time 15.

for regions that showed obvious and rapid changes in fluorescence. In most larvae, more than one such ROI could be identified, though sometimes this was not possible as the transgene showed some mosaicism, and sometimes larvae were damaged during loading (Figure S3). Note that because separate ROIs have been analyzed in the same larva, the set of images in Figures 7 and S3 includes some duplicate images but with separate ROIs identified. We were not able to identify individual cells within ROIs as the *DMRT* enhancer expresses quite broadly; however, their positioning relative to anatomical landmarks suggested their identity.

A small population of cells near the ocellus and otolith were found to synchronize with the flow protocol, with strong reporter activity coinciding with the CO_2 stimulus but not with the pH-matched control (Figure 7a–f). From their position, these could be aATEN epidermal

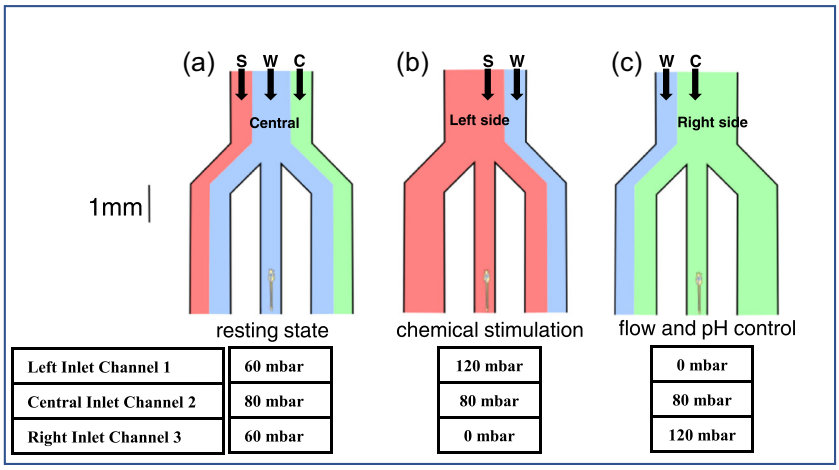

FIGURE 6 Experimental setup for exposing *Ciona intestinalis* larvae to CO_2-enriched sea water. This represents an expansion of the area outlined in Figure 3, showing the flow patterns used in the experimental protocol. Flow direction is from top to bottom. (a) In the resting state, the larva is exposed to a continuous flow of artificial sea water (W, in blue), while the stimulus (S, in red) and the flow control (C, in green) are flowing on the side streams. (b) During chemical stimulation, the flow boundaries move to hit the larva with the stimulus. (c) In flow control, the larva is instead hit with the control pH-matched stream. The pressure value for each inlet used to obtain the specific flow patterns is indicated at the bottom. Scale bar = 1 mm.

sensory neurons (Figure 1c). However, sensory vesicle neurons also lie under the aATENs in this area and we were not able to conclusively distinguish between these cell populations. When an ROI was drawn in the palp area (Figure 7h,i), reporter spikes were registered when stimulated by both increased CO_2 solution and the pH-matched control solution. Responsive cells were also seen positioned between the palps and sensory vesicle (Figure 7g), which could correspond to the position of RTENs, judging by published in situ hybridization data (Kusakabe et al., 2012). RTENs connect the palps to the sensory vesicle, so, if palp cells were detecting stimuli, we would expect this signal to pass via the RTENs. However, this remains speculative as we cannot be certain of cell identity without additional cell markers.

3 | DISCUSSION

3.1 | Live imaging of chemosensation in transgenic *C. intestinalis*

Small marine larvae such as those of *Ciona spcs*. offer the prospect of linking sensory input to individually identified cells. Here we report a step toward this goal with the immobilization of live transgenic larvae in a microfluidic chip and recording of cell activity while a specific stimulus is applied. Three technical developments were needed to support this, the development of an appropriate chip and fluid control system, the delivery of a transgene to the right cells, and imaging of informative fluorescence. Our chip design allows immobilization of multiple larvae and their exposure to three different fluid streams in a controlled manner. We did find some differences in the speed of onset on the left and right sides of the chip. In principle, the symmetric design should mean the two sides behave the same way, so this may be due to imprecision in the mold or variation in the tubing used to supply the solutions to the lateral streams. However, the speed of onset and offset on the two sides were internally relatively consistent.

We used this to examine larval sensitivity to dissolved CO_2. In total, we recorded Ca^{2+} transients in seven larval trunks while stimulating them with CO_2 and a pH-matched control solution and identified cells responding to these stimuli. The clearest specific response came from cells in or over the top of the sensory vesicle. Ca^{2+} levels in these cells precisely matched the onset and offset of the CO_2 stimulus but were not triggered by the pH-matched control. This shows the Ca^{2+} activity was caused by the elevated CO_2 in the test solution and not by the pH difference or mechanosensation of the change in stream. This is the first demonstration that *C. intestinalis* larvae can sense dissolved CO_2. We do not know what function this serves but can speculate it aids predator avoidance in the plankton and/or might help larvae identify a settlement site. To distinguish between these, it will be necessary to simultaneously image stimulus receipt and its response, in the form of effector neuron activity (e.g., motor neurons) and specific behaviors (such as muscle activity or triggering of metamorphosis). The cells responding to CO_2 in this instance might be aATENs (Figure 1) based on their position in the trunk and/or underlying neurons within the sensory vesicle. As aATENs project to this region of the sensory vesicle (Ryan et al., 2016), and if aATENs respond, we would expect neurons here to also respond. Distinguishing between these possibilities will be feasible using transgenic drivers specific to these cell types.

We also detected Ca^{2+} transients in the palps, but unlike aATENs, these responded to both stimulus and control solutions. This could reflect a response to pH and/or to mechanical force.

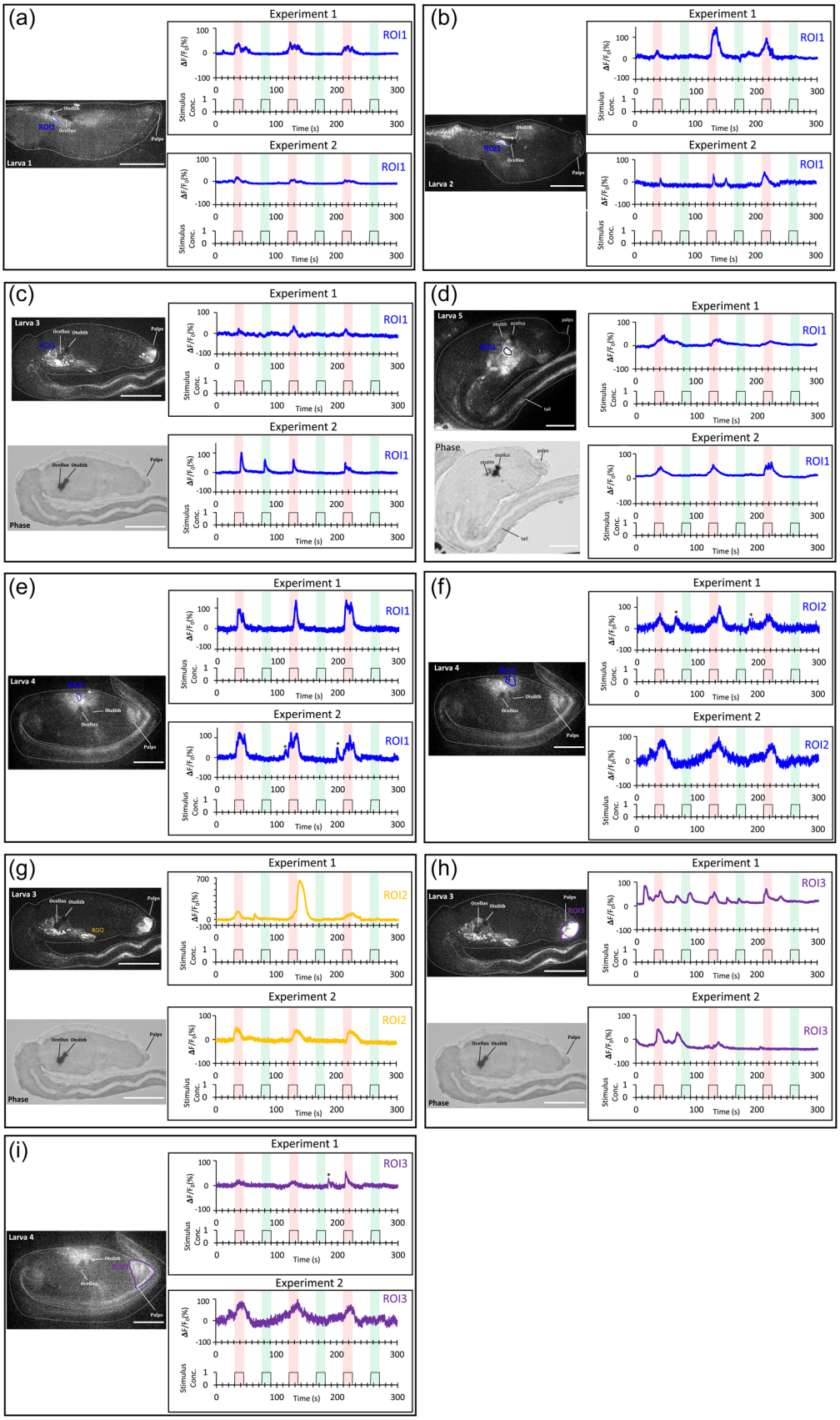

FIGURE 7 (See caption on next page).

Others have shown that the palps can detect mechanical stimuli and that this is part of the mechanism that initiates larval attachment and metamorphosis (Wakai et al., 2021). Finally, during stimulation, we detected Ca^{2+} transients in cells in the right position to be the RTENs. As RTENs relay sensory information from palps to sensory vesicle, their activity is likely caused by activity in the palps. However, as we only recorded activity from this area from one embryo and cannot be certain the responding cells are RTENs, this is suggestive only and needs further study.

There are limitations to our study. First, we have only imaged a small number of larvae. Second, while our study shows that GCaMP6m can be delivered to and recorded from a defined subset of cells, the *DMRT* enhancer has quite broad expression, so we were not able to conclusively identify specific cells. This could be solved using enhancers specific to cell types. It is also straightforward to introduce multiple transgenes simultaneously into *Ciona spcs*. so anatomically separated cells could be labelled and recorded at the same time. Third, challenges remain in chip design. Most notably *Ciona spcs*. larvae are soft-bodied and damage is possible on loading into the chip. While cells in damaged larvae remain alive and can be recorded, connections between nerve cells may be compromised. Integrating our design with suction mechanisms such as those recently described in a parallel study (Hoyer et al., 2024) might solve this. Fourth, while we demonstrate CO_2 responses we do not know their behavioral relevance. Overall, however, our protocol allows recordings from immobilized larvae at the resolution needed to identify the cells involved and will allow other olfactants to be tested, including those derived from biofilms from natural settlement sites and artificial structures like ship hulls.

4 | MATERIALS AND METHODS

4.1 | Animals and electroporation

Adult *C. intestinalis* (formerly known as *Ciona intestinalis* Type B) were collected from Northney Marina, Hayling Island, UK. They were maintained in a marine aquarium at 13°C and held under constant light to inhibit natural spawning. Gametes were removed by dissection and fertilization was performed in vitro. Within 15 min of fertilization, zygotes had their chorion and follicle cells removed (Mita-Miyazawa et al., 1985). They were then electroporated with plasmid DNA (Corbo et al., 1997). Transgenic embryos were raised at 18°C on agarose-coated Petri dishes in filtered sea water until they reached the desired stage for the experiment, that is, 20 h.

4.2 | *DMRT>GCaMP6m* construct design and validation

The regulatory region from *DMRT* (*C. robusta* gene ID: KH2012:KH.S544.3) was amplified from the *DMRT>GFP* plasmid (Wagner & Levine, 2012) using Phusion polymerase (New England Biolabs) with primers: 5′-ACGAGATCTTAGTAGGGTGGAGGAAGATGG-3′ and 5′-ACGCCTAGGGCCAGTTA-AACGAACTGTTTG-3′. The *DMRT* regulatory region was inserted into the plasmid pAAV-hSyn1-mRuby2-GSG-P2A-GCaMP6m-WPRE-pA (Addgene; #51473) cut with *Avr*II and *Bgl*II restriction enzymes. To validate GCaMP6m activity *C. intestinalis* larvae transgenic for *DMRT>GCaMP6m* were immobilized in low-melting point agarose inside a perfusion slide (μ-Slide Luer; ibidi) perfused with sea water. GCaMP6m was excited at 488 nm and fluorescence was detected with a Fluorescence Axio Zoom V.16 microscope, equipped with a Plan-NEOFLUAR Z ×2.3 (NA 0.57). GCaMP6m fluorescence was recorded for 30 s (300 frames at 10 frames/s). The slide was perfused with 1 M calcium ionophore A23187 diluted in sea water. GCaMP6m fluorescence was then also recorded for 30 s (300 frames at 10 frames/s). Identification of the responding cells was undertaken using Fiji by calculating the standard deviation through all 300 frames in both conditions. Note this imaging method differs from that used for embryos held in the microfluidic chip (see below) so fluorescent intensity in images cannot be directly compared.

4.3 | Microfluidic chip fabrication

Standard soft lithography was used to fabricate the mold (Xia & Whitesides, 1998). The photomask was designed with AutoCAD (2019 free student version; Autodesk Inc.). Premium-grade high-resolution film photomasks (features down to 5 μm) were printed by Micro Lithography Services Limited, Chelmsford, UK. The photomask source file is available as.dwg file (Additional File S1). The chip mold with a uniform height of 23.5 μm was obtained by spin coating a silicon wafer (4 in.; Siltronix) with a negative photoresist (SU-8 2035; MicroChem Corp.) according to the manufacturer's instructions. Devices were produced by pouring onto a mold a prepolymer mixture of polydimethylsiloxane (PDMS; Sylgard 184 silicone elastomer kit; Dow Corning Corp.) with a 1:10 ratio of curing agent and curing at 65°C for a minimum of 4 h.

FIGURE 7 Ca^{2+} imaging in *Dmrt>GcAMP6m* expressing cells. (a) Larva 1. (b) Larva 2. (c) Larva 3. (d) Larva 5. (e) Larva 4. (f) Larva 4. (g) Larva 3. (h) Larva 3. (i) Larva 4. The fluorescence images show the ROIs used to make the calcium activity traces. The graphs show the temporal patterns of fluorescence intensity for each region of interest (ROI). The red bar corresponds to exposure to the solution with high CO_2. The green bar is exposed to pH control. Asterisks mark calcium peaks happening outside the zone of chemical exposure (red). Note that (e), (f), and (i) are separate ROIs recorded for the same larva, as are (c), (g), and (h). Traces and ROIs are color-coded: blue indicates sensory vesicle and/or aATENs, orange indicates possible RTENs, and purple indicates palps. Two additional larvae are shown in Figure S3. Scale bars = 50 μm.

PDMS blocks were then irreversibly bound to a 1-mm-thick standard microscope slide (25 mm × 75 mm) by a 1-min treatment in a plasma oven. Occasionally bonding failed and these chips were not used. Other than that, problems with leaky chips were not encountered. Chips were also reused multiple times without signs of failure. We also tried bonding chips to coverslips, which also worked effectively, though we did not use these in subsequent experiments as they were not needed for imaging and were more fragile. A customized three-dimensional (3D)-printed chip holder was used to maintain the chip under an upright microscope. The chip holder source file is available as a.stl file (Additional File S2).

4.4 | Preparation of stimulus test solution

Artificial sea water (ASW) with a salinity level of 35 ppt, a carbonate hardness (dKH) of 8, and a pH of 8 was obtained by mixing 35 g of pharmaceutical-grade sea salt (PRO-REEF Sea Salt) per liter of ultrapure water. CO_2 was dissolved in ASW using a SodaStream with a built-in CO_2 cylinder. ASW with infused CO_2 had a lowered pH of 6. This decrease in pH relates to an estimated CO_2 concentration of 129.3 mg L^{-1} (ppm) in comparison to noninjected ASW at 1.1 mg L^{-1} (ppm) of CO_2, based on calculations from (Mojica Prieto & Millero, 2002). Due to the lowering effect of CO_2 on the pH, a control ASW solution was made with a corrected pH of 6 by adding 1 M HCl. The stock solutions were kept at 18°C in sealed glass bottles for long-term storage and loaded in 15 mL Falcon tubes on the day of the experiment to avoid possible detection of dissolved substances derived from plastic containers.

4.5 | Image analysis

GCaMP6m fluorescence excited at 488 nm wavelength was detected with a Fluorescence Axio Zoom V.16 microscope, equipped with a Plan-NEOFLUAR Z ×2.3 (NA 0.57). A total of 3000 images were taken at 10 fps (100 ms exposure time) in 300 s. A pixel binning of 5 × 5 was done to increase the signal-to-noise ratio. Movement artifacts on the raw calcium recordings were first corrected in FIJI (v.2.1.0) using the plugin TurboReg with rigid body transformations (Thevenaz et al., 1998). Mean fluorescence intensity was then calculated from each region of interest (ROI) drawn manually in FIJI. The attribution of an ROI to a specific embryonic region relied on its relative position guided by anatomical landmark recognition such as the palps, tail, ocellus, and otolith. Further data analysis was done in Excel, following the guidelines of Akira Muto (http://akiramuto.net/archives/148). Traces were plotted as $\Delta F/F_0 = (F_t - F_0)/F_0$, with F_t the fluorescence intensity at time t, and F_0 the mean fluorescence value over a 5-s time window during the initial 30 s resting state. The fluorescence change ($\Delta F/F_0$) was calculated after subtracting the background fluorescence.

ACKNOWLEDGMENTS

We thank Dr Laurence Lemaire and Professor Mike Levine for providing the *DMRT>GFP* construct. PDMS microfluidic chip fabrication was done in the laboratory of Professor Dirk Aarts (Oxford Colloid Group, Physical and Theoretical Chemistry, University of Oxford). Image acquisition was made with the kind help of Professor Mark Fricker (Department of Plant Sciences, University of Oxford). We are grateful to Northney Marina for allowing animal collection. We also acknowledge the John Fell Fund and the Elizabeth Hannah Jenkinson Fund, University of Oxford, for financial support.

CONFLICT OF INTEREST STATEMENT

The authors declare no conflict of interest.

DATA AVAILABILITY STATEMENT

Plasmid constructs generated in this study are available by request from the corresponding author. Design specifications for the microfluidic chip and chip holder are included with the manuscript as Additional Files S1 and S2. Additional File S3 is available on figshare (https://figshare.com/articles/media/Additional_File_3_Specimen_video_of_onset_avi/24039084). Raw imaging files of larval GCaMP recordings are available on figshare (https://figshare.com/articles/media/Ciona_larvae_imaged_for_GCaMP6m/24024729).

ORCID

Sebastian M. Shimeld http://orcid.org/0000-0003-0195-7536

PEER REVIEW

The peer review history for this article is available at https://www.webofscience.com/api/gateway/wos/peer-review/10.1002/jez.b.23267.

REFERENCES

Abdul-Wajid, S., Morales-Diaz, H., Khairallah, S. M., & Smith, W. C. (2015). T-type calcium channel regulation of neural tube closure and EphrinA/EPHA expression. *Cell Reports*, *13*, 829–839.

Abitua, P. B., Gainous, T. B., Kaczmarczyk, A. N., Winchell, C. J., Hudson, C., Kamata, K., Nakagawa, M., Tsuda, M., Kusakabe, T. G., & Levine, M. (2015). The pre-vertebrate origins of neurogenic placodes. *Nature*, *524*, 462–465.

Akahoshi, T., Hotta, K., & Oka, K. (2017). Characterization of calcium transients during early embryogenesis in ascidians *Ciona robusta* (*Ciona intestinalis* type A) and *Ciona savignyi*. *Developmental Biology*, *431*, 205–214.

Athira, A., Dondorp, D., Rudolf, J., Peytral, O., & Chatzigeorgiou, M. (2022). Comprehensive analysis of locomotion dynamics in the protochordate *Ciona intestinalis* reveals how neuromodulators flexibly shape its behavioral repertoire. *PLoS Biology*, *20*, e3001744.

Bostwick, M., Smith, E. L., Borba, C., Newman-Smith, E., Guleria, I., Kourakis, M. J., & Smith, W. C. (2020). Antagonistic inhibitory circuits integrate visual and gravitactic behaviors. *Current Biology*, *30*, 600–609.e2.

Chartier, T. F., Deschamps, J., Dürichen, W., Jékely, G., & Arendt, D. (2018). Whole-head recording of chemosensory activity in the marine annelid *Platynereis dumerilii*. *Open Biology*, *8*, 180139.

Chen, T. W., Wardill, T. J., Sun, Y., Pulver, S. R., Renninger, S. L., Baohan, A., Schreiter, E. R., Kerr, R. A., Orger, M. B., Jayaraman, V., Looger, L. L.,

Svoboda, K., & Kim, D. S. (2013). Ultrasensitive fluorescent proteins for imaging neuronal activity. *Nature*, *499*, 295–300.

Corbo, J. C., Levine, M., & Zeller, R. W. (1997). Characterization of a notochord-specific enhancer from the Brachyury promoter region of the ascidian, *Ciona intestinalis*. *Development*, *124*, 589–602.

Gainous, T. B., Wagner, E., & Levine, M. (2015). Diverse ETS transcription factors mediate FGF signaling in the Ciona anterior neural plate. *Developmental Biology*, *399*, 218–225.

Hackley, C., Mulholland, E., Kim, G. J., Newman-Smith, E., & Smith, W. C. (2013). A transiently expressed connexin is essential for anterior neural plate development in *Ciona intestinalis*. *Development*, *140*, 147–155.

Hadfield, M. G. (2011). Biofilms and marine invertebrate larvae: What bacteria produce that larvae use to choose settlement sites. *Annual Review of Marine Science*, *3*, 453–470.

Hoyer, J., Kolar, K., Athira, A., van den Burgh, M., Dondorp, D., Liang, Z., & Chatzigeorgiou, M. (2024). Polymodal sensory perception drives settlement and metamorphosis of Ciona larvae. *Current Biology*, *34*, 1168–1182.e7.

Imai, J. H., & Meinertzhagen, I. A. (2007). Neurons of the ascidian larval nervous system in *Ciona intestinalis*: II. Peripheral nervous system. *Journal of Comparative Neurology*, *501*, 335–352.

Johnson, C. J., Razy-Krajka, F., & Stolfi, A. (2020). Expression of smooth muscle-like effectors and core cardiomyocyte regulators in the contractile papillae of Ciona. *EvoDevo*, *11*, 15.

Jones, W. (2013). Olfactory carbon dioxide detection by insects and other animals. *Molecules and Cells*, *35*, 87–92.

Kolar, K., Dondorp, D., Zwiggelaar, J. C., Høyer, J., & Chatzigeorgiou, M. (2021). Mesmerize is a dynamically adaptable user-friendly analysis platform for 2D and 3D calcium imaging data. *Nature Communications*, *12*, 6569.

Kourakis, M. J., Borba, C., Zhang, A., Newman-Smith, E., Salas, P., Manjunath, B., & Smith, W. C. (2019). Parallel visual circuitry in a basal chordate. *eLife*, *8*, e44753.

Kusakabe, T. G., Sakai, T., Aoyama, M., Kitajima, Y., Miyamoto, Y., Takigawa, T., Daido, Y., Fujiwara, K., Terashima, Y., Sugiuchi, Y., Matassi, G., Yagisawa, H., Park, M. K., Satake, H., & Tsuda, M. (2012). A conserved non-reproductive GnRH system in chordates. *PLoS One*, *7*, e41955.

Mita-Miyazawa, I., Ikegami, S., & Satoh, N. (1985). Histospecific acetylcholinesterase development in the presumptive muscle cells isolated from 16-cell-stage ascidian embryos with respect to the number of DNA replications. *Development*, *87*, 1–12.

Mojica Prieto, F. J., & Millero, F. J. (2002). The values of pK1 + pK2 for the dissociation of carbonic acid in seawater. *Geochimica et Cosmochimica Acta*, *66*, 2529–2540.

Nicol, D., & Meinertzhagen, I. A. (1991). Cell counts and maps in the larval central nervous system of the ascidian *Ciona intestinalis* (L.). *Journal of Comparative Neurology*, *309*, 415–429.

Okawa, N., Shimai, K., Ohnishi, K., Ohkura, M., Nakai, J., Horie, T., Kuhara, A., & Kusakabe, T. G. (2020). Cellular identity and Ca(2+) signaling activity of the non-reproductive GnRH system in the *Ciona intestinalis* type A (*Ciona robusta*) larva. *Scientific Reports*, *10*, 18590.

Pennati, R., Groppelli, S., De Bernardi, F., Mastrototaro, F., & Zega, G. (2009). Immunohistochemical analysis of adhesive papillae of *Clavelina lepadiformis* (Müller, 1776) and *Clavelina phlegraea* (Salfi, 1929) (Tunicata, Ascidiacea). *European Journal of Histochemistry*, *53*, 4.

Poncelet, G., & Shimeld, S. M. (2020). The evolutionary origins of the vertebrate olfactory system. *Open Biology*, *10*, 200330.

Ryan, K., Lu, Z., & Meinertzhagen, I. A. (2016). The CNS connectome of a tadpole larva of *Ciona intestinalis* (L.) highlights sidedness in the brain of a chordate sibling. *eLife*, *5*, e16962.

Scott, K. (2011). Out of thin air: Sensory detection of oxygen and carbon dioxide. *Neuron*, *69*, 194–202.

Thevenaz, P., Ruttimann, U. E., & Unser, M. (1998). A pyramid approach to subpixel registration based on intensity. *IEEE Transactions on Image Processing*, *7*, 27–41.

Tresser, J., Chiba, S., Veeman, M., El-Nachef, D., Newman-Smith, E., Horie, T., Tsuda, M., & Smith, W. C. (2010). Doublesex/mab3 related-1 (dmrt1) is essential for development of anterior neural plate derivatives in Ciona. *Development*, *137*, 2197–2203.

Tsuda, M., Sakurai, D., & Goda, M. (2003). Direct evidence for the role of pigment cells in the brain of ascidian larvae by laser ablation. *Journal of Experimental Biology*, *206*, 1409–1417.

Wagner, E., & Levine, M. (2012). FGF signaling establishes the anterior border of the Ciona neural tube. *Development*, *139*, 2351–2359.

Wakai, M. K., Nakamura, M. J., Sawai, S., Hotta, K., & Oka, K. (2021). Two-round Ca(2+) transient in papillae by mechanical stimulation induces metamorphosis in the ascidian *Ciona intestinalis* type A. *Proceedings. Biological Sciences*, *288*, 20203207.

Xia, Y., & Whitesides, G. M. (1998). Soft lithography. *Angewandte Chemie International Edition*, *37*, 550–575.

Yokoyama, T. D., Hotta, K., & Oka, K. (2014). Comprehensive morphological analysis of individual peripheral neuron dendritic arbors in ascidian larvae using the photoconvertible protein Kaede. *Developmental Dynamics*, *243*, 1362–1373.

Zeng, F., Wunderer, J., Salvenmoser, W., Hess, M. W., Ladurner, P., & Rothbächer, U. (2019). Papillae revisited and the nature of the adhesive secreting collocytes. *Developmental Biology*, *448*, 183–198.

SUPPORTING INFORMATION

Additional supporting information can be found online in the Supporting Information section at the end of this article.

How to cite this article: Poncelet, G., Parolini, L., & Shimeld, S. M. (2024). A microfluidic chip for immobilization and imaging of *Ciona intestinalis* larvae. *Journal of Experimental Zoology Part B: Molecular and Developmental Evolution*, *342*, 443–452. https://doi.org/10.1002/jez.b.23267